Author(s): Maaninen, Tiina; Tuononen, Heikki; Kosunen, Katja; Oilunkaniemi, Raija; Hiitola, Johanna; Laitinen, Risto; Chivers, Tristram

Title: Formation, Structural Characterization, and Calculated NMR Chemical Shifts of Selenium-Nitrogen Compounds from SeCl4 and ArNHLi (Ar = supermesityl, mesityl)

Year: 2004

Version:

Please cite the original version:

Maaninen, T., Tuononen, H., Kosunen, K., Oilunkaniemi, R., Hiitola, J., Laitinen, R., & Chivers, T. (2004). Formation, Structural Characterization, and Calculated NMR Chemical Shifts of Selenium-Nitrogen Compounds from SeCl4 and ArNHLi (Ar = supermesityl, mesityl). Zeitschrift für Anorganische und Allgemeine Chemie, 630(12), 1947-1954. https://doi.org/10.1002/zaac.200400286

Formation, Structural Characterization, and Calculated NMR Chemical Shifts of Selenium-Nitrogen Compounds from $SeCl_4$ and ArNHLi (Ar = supermesityl, mesityl)

Tiina Maaninen,[a] Heikki M. Tuononen,[b] Katja Kosunen,[a] Raija Oilunkaniemi,[a] Johanna Hiitola,[a] Risto Laitinen,[a]* and Tristram Chivers [c]

[a] Oulu, Department of Chemistry, University of Oulu, Finland

[b] Jyväskylä, Department of Chemistry, University of Jyväskylä, Finland

[c] Calgary, Department of Chemistry, University of Calgary, Canada

* Prof. Risto S. Laitinen
Department of Chemistry
P.O. Box 3000
FIN-90014 University of Oulu
Finland
Tel. +358-8-553-1611
Fax. +358-8-553-1608
E-mail: risto.laitinen@oulu.fi

Abstract

Supermesityl selenium diimide [Se{N($C_6H_2{}^tBu_3$-2,4,6)}$_2$; Se{N(mes*)}$_2$] can be prepared in a good yield from the reaction of $SeCl_4$ and (mes*)NHLi. The molecule adopts an unprecedented *anti,anti*-conformation, as deduced by DFT calculations at PBEO/TZVP level of theory and supported by ^{77}Se NMR spectroscopy and a crystal structure determination. An analogous reaction involving ($C_6H_2Me_3$-2,4,6)NHLi [(mes)NHLi] unexpectedly lead to the reduction of selenium and afforded the selenium diamide Se{NH(mes)}$_2$ that was characterized by X-ray crystallography and ^{77}Se NMR spectroscopy. The Se-N bonds of 1.847(3) and 1.852(3) Å show normal single bond lengths. The <NSeN bond angle of 109.9(1) ^{o} also indicates a tetrahedral AX_2E_2 bonding arrangement around selenium. Two N-H···N hydrogen bonds link the Se{NH(mes)}$_2$ molecule with two discrete (mes)NH_2 molecules. In the solid state selenium diamide adopts the *anti*-conformation, while in solution the presence of both *syn*- and *anti*-isomers could be observed. PBEO/TZVP calculations of the shielding tensors of 28 different types of selenium-containing molecules, for which the ^{77}Se chemical shifts are unambiguously known, were carried out to assist the spectral assignment of Se{N(mes*)}$_2$ and Se{NH(mes)}$_2$.

Key words: selenium(IV) diimides, selenium(II) diamides, X-ray crystallography, NMR spectroscopy, DFT calculations

Introduction

Selenium diimides have been known for over 25 years [1]. Unlike sulfur diimides that are stable compounds and find extensive use as ligands in transition metal complexes [2-4] and reagents in organic and inorganic syntheses [5,6], selenium diimides are thermally unstable [1,7-9] and have therefore more limited applications. They are, however, efficient *in situ* reagents for allylic amination of olefins and 1,2-diamination of 1,3-dienes [1,10]. *tert*-Butyl selenium diimide also forms an *N*,*N*′-chelated adduct with $SnCl_2$ [11] and has been used to generate the dianion $Se(N^tBu)_3^{2-}$ that is isoelectronic with SeO_3^{2-} [12].

It has been shown by X-ray crystallography in the solid state and by electron diffraction in the gas phase that different sulfur diimides exhibit either *syn,anti* or *syn,syn* conformations depending on the organic substituent [13]. The structural information for selenium diimides is much sparser. Herberhold *et al.* [7,8] have deduced on the basis of NMR spectroscopy that in solution $Se(N^tBu)_2$ is in *syn,anti* conformation. The X-ray structure of adamantyl selenium diimide also shows a *syn,anti* conformation [14].

It is well-established that sulfur diimides exclusively exist as monomeric species [13]. By contrast, *tert*-butyl tellurium diimide is dimeric both in solution and in solid state [15-17]. Recent MO calculations at different levels of theory [13,18] have predicted that the [2+2] cyclodimerization reactions of sulfur diimides are endothermic and those of tellurium diimides are exothermic. In the case of selenium diimides, the most reliable calculations imply that the energy change in the cyclodimerization is slightly positive [13,18]. This is consistent with the observed monomeric structures both in solution and in the solid state [8,14]. Only in the case of trimethylsilyl selenium diimide are there some indications that the species may be dimeric in solution [9,13,19].

A convenient method to prepare selenium diimides is a direct reaction between selenium tetrachloride and a primary amine [7,l4,20]. In case of tellurium diimide dimers, the amine was lithiated prior to the reaction with tellurium tetrachloride [15-17]. In the present work we explored the reactions of 2,4,6-$^{t}Bu_3C_6H_2NHLi$ [(mes*)NHLi] and 2,4,6-$Me_3C_6H_2NHLi$ [(mes)NHLi] with $SeCl_4$. (mes*)NHLi produced $Se\{N(mes^*)\}_2$ (**1**) in which the molecule exhibits an unprecedented *anti,anti*-conformation. The treatment of (mes)NHLi with $SeCl_4$ unexpectedly yielded mesityl selenium diamide $Se\{NH(mes)\}_2$ (**2**). The products were characterized by X-ray crystallography and NMR spectroscopy. We also report DFT calculations of the ^{77}Se chemical shifts of various Se-containing species that were carried out to assist the assignment of the ^{77}Se NMR spectra of the new species prepared in this work.

Results and Discussion

Synthesis of $Se\{N(mes^*)\}_2$ (1) and $Se\{NH(mes)\}_2$ (2)

The lithiation of supermesityl amine with *n*-BuLi followed by the treatment with $SeCl_4$ expectedly afforded supermesityl selenium(IV) diimide (**1**).

$$4\ (mes^*)NHLi + SeCl_4 \longrightarrow Se\{N(mes^*)\}_2 + 2\ (mes^*)NH_2 + 4\ LiCl \qquad (1)$$

Only one resonance at 1844 ppm was observed in the ^{77}Se NMR spectrum of the reaction mixture. It is found in a region typical for selenium diimides and is assigned to **1**.

By contrast, the analogous reaction involving mesityl amine unexpectedly lead to the reduction of selenium and afforded a novel amide containing two Se-N single bonds:

$$4\ (mes)NHLi + SeCl_4 \longrightarrow Se\{NH(mes)\}_2 + ½\ (mes)N{=}N(mes) + (mes)NH_2 + 4\ LiCl \quad (2)$$

The ^{77}Se NMR spectrum of the reaction mixture shows two close-lying resonances of equal intensity at 1077 and 1076 ppm. They are assigned to two isomers of **2** (see discussion below). The formation of the three nitrogen-containing compounds could be detected by ^{14}N NMR spectroscopy. The resonance at -333 ppm is due to $(mes)NH_2$. The resonance at 160 ppm is assigned to (mes)N=N(mes). It expectedly lies downfield from the resonance of PhN=NPh for which the ^{15}N chemical shift has been reported at 118.7 ppm [21]. The third resonance is observed at –71 ppm and is assigned to $Se\{(mes)NH\}_2$ (**2**).

The difference in the reactivity upon treatment of (mes*)NHLi or (mes)NHLi with $SeCl_4$ is very striking, since supermesityl and mesityl groups are electronically rather similar. The former species yields quantitatively supermesityl selenium(IV) diimide (**1**), while the latter species results in the reduction of $SeCl_4$ with the production of mesityl selenium(II) diamide (**2**). At present the reason for this difference is not clear, but we note that Björgvinsson *et al.* [22] have observed a similar reduction when treating $LiN(SiMe_3)_2$ with $TeCl_4$. In this reaction $Te\{N(SiMe_3)_2\}_2$ is formed.

Molecular Structures of $Se\{N(mes^*)\}_2$ and $Se\{NH(mes)\}_2 \cdot 2(mes)NH_2$

Like all chalcogen diimide monomers, supermesityl selenium diimide (**1**) can have three possible conformations:

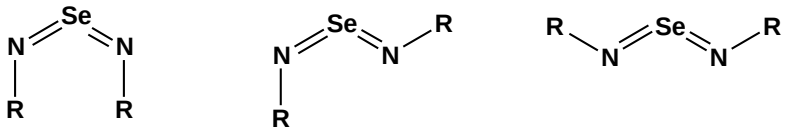

syn,syn *syn,anti* *anti,anti*

It has been well-established by recent MO calculations that for a majority of sulfur and selenium diimides the *syn,anti* and *syn,syn* conformations lie lower in energy than the *anti,anti* conformations [13,18]. In case of **1**, however, the *anti,anti* conformation is found to be energetically most favourable at PBE0/TZVP level of theory, though the *syn,anti* and *syn,syn* conformations lie only 11 and 10 kJ mol^{-1} higher in energy, respectively. An approximate crystal structure determination of a poor quality crystal of $Se\{N(mes^*)\}_2$ has indeed established that the molecule exhibits the *anti,anti* conformation [see Figure 1(a)].* It is interesting to note that in the solid state $S\{N(mes^*)\}_2$ is known to lie in the *syn,anti* conformation [23].

The PBE0/TZVP optimized geometries of the three conformations of **1** are shown in Figure 1. The lengths of the Se-N bonds indicate significant □-bonding and agree well with available experimental evidence from adamantyl selenium diimide [14]. While the corresponding bond lengths in all three conformations are virtually identical, the bond angles show a significant trend. The <N-Se-N and <Se-N-C bond angles become larger and more strained in the order *anti,anti* < *syn,anti* < *syn,syn* indicating that steric effects play a significant role in the optimized geometry of the three different conformations. It also

* Crystal data for **1**: $C_{18}H_{29}NSe_{0.50}$, M = 298.90, dark brown plates (0.20 x 0.12 x 0.08 mm^3), monoclinic, space group $C2/c$, a = 13.774(3), b = 13.889(3), c = 18.868(4) Å, β = 108.80(3)°, V = 3417(1) $Å^3$, Z = 8, ρ calcd = 1.162 g cm^{-3}, $\mu(MoK_\alpha)$ = 1.124 mm^{-1}, T = 150(2) K, $F(000)$ = 1288. Total no. of reflections 18465 (2985 unique). R_1 = 0.1505 and wR_2 = 0.4366 [2583 reflections with $I_o > 2\sigma(I_o)$], R_1 = 0.1622 and wR_2 = 0.4432 (all data).

explains the unexpected observation that the *anti,anti* conformation is energetically most favourable. The experimental bond parameters from our tentative crystal structure determination are also shown in Figure 1(a). They are in very good agreement with the calculated values. The PBE0/TZVP optimized structure and the crystal structure also show very similar relative orientations between the two phenyl rings.

The molecular structure of $Se\{NH(mes)\}_2 \cdot 2(mes)NH_2$ is shown in Figure 2 and the selected bond lengths in Table 1. The Se-N bond of 1.847(3)-1.852(3) Å exhibits an approximate single bond length {*c.f.* 1.869(2) Å in $Se\{N(SiMe_3)_2\}_2$ [22]} the <N-Se-N bond angle of 109.9(1) ^{o} being consistent with the tetrahedral AX_2E_2 bonding arrangement of selenium. The hydrogen atoms H1 and H2 could be located from the difference Fourier map and their locations could be refined isotropically. The N1-H1 and N2-H2 bond lengths are 0.75(5) and 0.81(5) Å, respectively. The values are quite normal for N-H bonds. These hydrogen atoms are involved in hydrogen bonding to two discrete mesitylamine molecules as also shown in Figure 2. The two N···H contacts are 2.32(5) and 2.46(5) Å with the angles around H1 and H2 150(5) and 159(4) ^{o}. These values are quite typical for the hydrogen bonding arrangement involving nitrogen.

$Se\{NH(mes)\}_2$ (**2**) can have two possible isomers depending on the bonding arrangement around the two pyramidal nitrogen atoms, as shown in Figure 3. It can be seen that though the amino groups can rotate freely about the Se-N single bonds, these isomers are different entities. For convenience, the isomer shown in Figure 3(a) is referred to as the *syn*-isomer and that in Figure 3(b) is referred to as the *anti*-isomer, though these terms are rigorously defined only at limited ranges of the torsional angles about the Se-N bond. The selected optimized bond parameters calculated at the PBE0/TZVP level of theory are shown in Table 1 together with the experimental values from the crystal structure.

In the crystalline phase the *anti*-isomer of **2** is observed (see Table 1 and Figure 2). This can clearly be deduced by the signs of the torsional angles. Other bond parameters seem to be insensitive to the actual isomer. The optimized and experimental values agree well with each other. It is also interesting to note that though the free rotation of the amino group can be assumed *a priori*, the experimental torsional angles <N-Se-N-H and <N-Se-N-C from the crystal structure are rather close to the optimized values indicating that the intermolecular interactions in the solid phase play a minor role in determining the actual conformation of the molecule.

^{77}Se NMR Chemical Shifts

In NMR experiments, shielding constants are always measured relative to an appropriate reference system and the differences are reported as the nuclear chemical shifts δ. Theoretical calculations, on the other hand, give absolute shielding tensors σ and their traces $\sigma_{iso.}$. To a good approximation, the relationship between NMR chemical shifts and isotropic shieldings is

$$\delta = \sigma_{ref.} - \sigma_{iso.}, \qquad (3)$$

where $\sigma_{ref.}$ is the isotropic shielding of an appropriate reference system. A straightforward application of Eq. (1) in theoretical calculations does not, however, represent the best practical approach, as it assigns excessive significance to the error in the calculated shielding of the reference system, $\sigma_{ref.}$. For example, in the case of selenium NMR, the calculated chemical shift for the reference compound, dimethyl selenide, is highly dependent on the conformation, since the three possible conformations span a range of 80 ppm [24]. We have

therefore chosen to determine the $\sigma_{ref.}$ value used in Eq. (1) in such a way that the average absolute error in all calculated chemical shifts will be zero. This was done by forming a linear regression line between experimental chemical shift δ and calculated isotropic shielding $\sigma_{iso.}$ (see Figure 4).

The experimental ^{77}Se chemical shifts of Se-N compounds are found in a relatively narrow range between 800 ppm and 1500 ppm. This range is quite small considering that the experimentally observed ^{77}Se chemical shifts of all possible selenium compounds span a range of over 3000 ppm. Consequently, the determination of the $\sigma_{ref.}$ value by linear regression was made using a larger data set of selenium molecules and ions, the observed chemical shifts of which lie between -666 ppm and 2131 ppm. The calculated set included 28 selenium compounds that are listed in Table 2.

The geometries of the selected 28 selenium compounds were optimized at PBE0/TZVP level of theory. A remarkably good agreement between calculated and experimental geometries can be noted, as exemplified in Figure 1 for $Se\{N(mes^*)\}_2$ and Table 1 for $Se\{NH(mes)\}_2$. The RMS deviation of 20 different selenium-nitrogen single and double bond lengths is only 0.011 Å and that of 25 different bond angles involving selenium and nitrogen is 1.3 °. The consistency between experimental and calculated geometries is especially good for diimides and acyclic amines, and slightly worse for cyclic systems *e.g.* $Se_6(N^tBu)_2$ and $Se_9(N^tBu)_6$.

The isotropic shielding tensors were calculated on the optimized geometries and are shown in Table 2 along with their corresponding calculated and experimental ^{77}Se chemical shifts. Least squares refinement between experimental chemical shifts and calculated isotropic shieldings gave the following regression line (see Figure 4):

$$\delta = 1863.4 - 1.01\sigma_{iso} . \qquad (4)$$

The linear correlation coefficient is 0.997, which together with the almost unit slope shows that the fit between calculated shieldings and experimental chemical shifts is extremely good in the current case. This is a clear indication of the good performance of the PBE0 functional in prediction of magnetic properties.

The calculated mean deviation between calculated and experimental chemical shifts amounts to 48 ppm for the 32 different chemical shifts shown in Table 2. This is 10-30 ppm smaller than the values at the BP86 HF, and MP2 levels of theory [24,25]. It should be noted, however, that the previously reported mean deviations have been obtained using a much smaller set of selenium compounds and are therefore not strictly comparable with the present values. Since in general the effect of different solvents on the ^{77}Se chemical shift is of the order 20-30 ppm, the current method clearly approaches the limit of accuracy of theoretical calculations that are performed on single molecules in gas phase.

Despite the extremely good linearity of the fit and the low mean deviation, the absolute errors for some calculated chemical shifts are high being of the order of 100 ppm. The largest deviations are found for the cyclic Se-N systems $OSe(N^tBu)_2SeO$, $OSe(NAd)_2SeO$, $Se_3(N^tBu)_3$, and $Se_6(N^tBu)_2$. Most likely these errors arise from the differences in calculated optimum geometries and experimental geometries in solution. It is well known that the chemical shifts in general, and ^{77}Se chemical shifts in particular, are very sensitive to the geometry (see discussion of $SeMe_2$ [24]). This assumption was tested by calculating the NMR shielding tensors for $OSe(N^tBu)_2SeO$, $Se_3(N^tBu)_3$ and $Se_6(N^tBu)_2$ also in their experimentally observed geometries. The effect of geometry on the calculated ^{77}Se chemical shifts was indeed found to be substantial: Chemical shifts calculated at the experimental

geometries are 1110 ppm for $OSe(N^tBu)_2SeO$, 1162 ppm for $Se_3(N^tBu)_3$, and 1006 and 544 ppm for $Se_6(N^tBu)_2$. All shifts are moved downfield, which in general makes errors even larger. The largest error is now found for $Se_3(N^tBu)_3$ (234 ppm).

It is evident from above that there is a clear need to incorporate solvent effects into the theoretical model. The current approach to use geometries optimized in the gas phase represents a compromise between accuracy and computational cost. The largest calculated systems $Se_9(N^tBu)_6$ and $Se\{N(mes^*)\}_2$ use over 1000 basis functions which by itself makes even DFT calculations extremely time consuming. The inclusion of solvent model during geometry optimization would have been possible only by reducing the size of the basis set. For the semi-quantitative purposes that are aimed at the assignment of experimental ^{77}Se chemical shifts, the present method provides a sufficient accuracy.

The calculated PBE0/TZVP(P)//PBE0/TZVP isotropic shielding tensors and ^{77}Se chemical shifts of $Se\{N(mes^*)\}_2$ and $Se\{NH(mes\}\}_2$ are shown in Table 3. Since the objective is to use the computed chemical shifts in the assignment of the ^{77}Se NMR resonances of the two species, the shielding tensors have not been used in the creation of the linear regression line shown in Figure 4. Rather, this calibration line has been utilized in the determination of the chemical shifts.

The calculated ^{77}Se chemical shift of **1** is strongly dependent on the conformation of the molecule (see Table 3). The resonance of the *anti,anti*-conformation appears to be most deshielded and should be found at the lowest field. The chemical shift of the *syn,anti*-conformation lies next upfield and that of the *syn,syn*-conformation is found at the highest field.

The experimental ^{77}Se resonance of **1** is recorded from the THF solution at 25^{o}C and is observed at 1844 ppm. It can be seen from Table 3 that this value is approximately an average of the calculated chemical shifts of the *anti,anti*- and *syn,anti*-conformations and significantly larger than the value calculated for the *syn,syn*-conformation. The presence of the *syn,syn*-conformation can therefore clearly be ruled out. The choice between the *anti,anti*- and *syn,anti*-conformations can be made as follows:

The approximate crystal structure determination has established the presence of the *anti,anti*-conformation of **1** in the solid state. The two previously known selenium diimides, Se(N^{t}Bu)$_2$ [7,8] and Se(NAd)$_2$ [14] that exist in *syn,anti*-conformations show no evidence of interconversion between the conformations in solution. It is therefore probable that the solid state conformation of supermesityl selenium diimide (**1**) is also retained in solution. Furthermore, it can be seen from Table 2 that for both Se(N^{t}Bu)$_2$ and Se(NAd)$_2$, the computed prediction overestimates the experimental chemical shift. When all these observations are taken into account, it can be considered more likely that the experimental chemical shift of 1844 ppm represents the *anti,anti*-conformation of Se{N(mes*)}$_2$ rather than the *syn,anti*-conformation.

The ^{77}Se NMR spectrum of **2** in THF at 25^{o}C shows two close-lying resonances of equal intensity at 1077 and 1076 ppm. As seen from Table 3, the PBE0/TZVP(P)//PBE0/TZVP calculations predict the chemical shifts of *syn*- and *anti*-Se{NH(mes)}$_2$ at 1067 and 1066 ppm, respectively. It is therefore likely that both isomers exist in solution and that the observed resonance at 1077 ppm can be assigned to the *anti*-isomer and that at 1076 ppm to the *syn*-isomer. Upon crystallization, only the *anti*-isomer was isolated in the present work.

Experimental

General

All manipulations involving air-sensitive materials were conducted under an argon atmosphere by using Schlenk techniques or in a drybox. Solvents were dried and distilled under an argon atmosphere prior to use: tetrahydrofuran (THF) and diethylether over Na/benzophenone. $SeCl_4$, mesitylamine, and supermesitylamine (Aldrich) were used without further purification.

Instrumentation

The ^{13}C, ^{14}N, and ^{77}Se NMR spectra were recorded on a Bruker AM-400 or a Bruker DPX-400 spectrometer operating at 100.614, 28.915, and 76.312 MHz, respectively. The spectral widths were 23.81, 29.41, and 100.00 kHz, yielding the respective resolutions of 1.45, 3.59, and 6.10 Hz/data point. The ^{13}C pulse width was 3.50 μs, for ^{14}N 20.0 μs, and for ^{77}Se 9.00 μs. The ^{13}C, ^{14}N, and ^{77}Se accumulations contained 1000-20000, 20000-200000, and 15000-30000 transients, respectively. Relaxation delays were ^{13}C 3.0 s, ^{14}N 1 ms, and ^{77}Se 2.0 s. The ^{13}C chemical shifts are reported relative to TMS and the ^{14}N chemical shifts are reported relative to neat CH_3NO_2. The ^{77}Se NMR spectra were referenced externally to a saturated solution of SeO_2 in D_2O at room temperature. The chemical shifts are reported relative to neat Me_2Se at room temperature [$\delta(Me_2Se) = \delta(SeO_2) + 1302.6$] [29].

Preparation of Se{N(mes*)}$_2$ (1)

Supermesitylamine (2 mmol, 0.523 g) was dissolved in 20 cm^3 diethyl ether at -80°C and 2 cm^3 of 1M *n*-BuLi in hexanes (2 mmol) was added into the resulting solution. The reaction mixture was stirred for 20 min and was subsequently allowed to warm to the room temperature upon further stirring for 40 min. Diethyl ether was evaporated under vacuum, and the resulting white solid was dissolved in 20 cm^3 of tetrahydrofuran (THF). $SeCl_4$ (0.110 g, 0.5 mmol), dissolved in 5 cm^3 of THF) was added into the resulting solution at -80 ^{o}C. A black reaction mixture was formed and was allowed to warm slowly to the room temperature during stirring for 16 h. The solvent was evaporated under vacuum, and the product was dissolved in 15 cm^3 of hexane. The precipitate consisting of supermesitylammonium chloride and lithium chloride was removed upon filtration. The solvent was removed by evaporation. Recrystallization of the product from THF afforded black crystals of supermesitylselenium diimide (0.269 g, 90 %). Anal. calcd. for $C_{36}H_{58}N_2Se$: C 72.33, H 9.78, N 4.69; found C 72.30, H 9.40, N 5.52. ^{77}Se NMR (THF, 25 ^{o}C) δ = 1844 ppm.

Preparation of Se{NH(mes}$_2$·2(mes)NH$_2$ {2·2(mes)NH$_2$}

Mesitylamine (1.6 cm^3, 12.0 mmol) was dissolved in 40 cm^3 of diethyl ether and 12 cm^3 of 1 M *n*-BuLi in hexanes (12.0 mmol) was added at -80°C. The reaction mixture was stirred for 20 min and was then allowed to warm to room temperature upon further stirring for 40 min. The solvent was evaporated under vacuum and the resulting pale yellow solid was dissolved in 30 cm^3 of THF. $SeCl_4$ (0.662 g, 3 mmol) dissolved in 10 cm^3 of THF was added at -80 ^{o}C. A dark brown-red reaction mixture was formed that was allowed to warm slowly to room temperature upon stirring for 16 h stirring. The solvent was evaporated under vacuum, and the product was dissolved in 20 cm^3 of hexane. The lithium chloride precipitate was removed

by filtration. A dark brown-red oil was obtained when hexane was evaporated. Recrystallization from THF afforded dark red crystals of ***2***·2(mes)NH_2 embedded in oily material. Attempts to remove the crystals from oil resulted in rapid decomposition even under an argon atmosphere precluding satisfactory elemental analysis. ^{77}Se NMR (THF, 25 ^{o}C) δ = 1077, 1076 ppm.

X-ray Crystallography

Diffraction data for ***2***·2(mes)NH_2 were collected on a Nonius Kappa CCD diffractometer at 150 K using graphite monochromated MoK_α radiation (λ = 0.71073 Å). Crystal data and the details of structure determination are given in Table 4.

The structure was solved by direct methods using SHELXS-97 [30] and refined using SHELXL-97 [31]. After the full-matrix least-squares refinement of the non-hydrogen atoms with anisotropic thermal parameters, the hydrogen atoms were placed in calculated positions in the aromatic rings (C-H = 0.95 Å) and in the CH_3 groups (C-H = 0.99 Å). In the final refinement the hydrogen atoms were riding with the carbon atom they were bonded to. The isotropic thermal parameters of the hydrogen atoms were fixed at 1.2 and 1.5 times to that of the corresponding aromatic and aliphatic carbon atoms, respectively. The scattering factors for the neutral atoms were those incorporated with the programs.

Computational Details

In addition to Se{N(mes*)}$_2$ (**1**) and Se{NH(mes)}$_2$ (**2**) characterized in this work, the theoretical ^{77}Se shielding tensors were computed for 28 compounds for which the

experimental ^{77}Se chemical shift data are available (see Table 2). Geometries of all compounds were fully optimized at DFT level of theory using the PBE0 exchange-correlation hybrid functional and Ahlrichs' triple-zeta valence basis set augmented by one set of polarization functions (denoted TZVP). The PBE0 hybrid density functional [32-34] was chosen on the grounds of several published benchmarks that have shown its good performance in calculating molecular properties for a wide variety of chemical systems [34-37]. In particular, it has recently been shown to generally outperform the more popular B3LYP functional in the calculation of NMR chemical shifts for organic systems (especially ^{13}C, ^{15}N and ^{17}O nuclei) [35,36]. The way in which the PBE0 functional is constructed and the lack of empirical parameters fitted to specific physical properties makes it more appealing also from a purely theoretical viewpoint.

Tight optimization criteria with energy convergence of 10^{-7} a.u. and gradient norm convergence of 10^{-4} a.u. were imposed to ensure that fully converged geometric parameters are obtained. Experimental crystal structures [14,20,22,23,38] were used as starting guesses for geometry optimizations where available and appropriate point group symmetries were utilized in order to speed up calculations. Fundamental vibrations were calculated to establish that the optimized geometries represent local minima.

Nuclear magnetic shielding tensors were calculated for each stationary point employing the GIAO [39] method and PBE0 functional. For NMR calculations, the basis set was further augmented using polarization functions from the TZVPP basis set on selenium atoms and all other atoms directly bonded to selenium. The used locally dense basis set, denoted hereafter as TZVP(P), is therefore TZVPP quality around the selenium nuclei and TZVP for any other element.

All geometry optimizations were carried out with a Turbomole 5.6 program package [40-42] due to its efficient parallelization and ability to use also non-Abelian point groups. However, nuclear magnetic shielding tensors were calculated with Gaussian 03 [43], since the current implementation of Turbomole lacks support for the PBE0 functional. Both atomic basis sets TZVP and TZVPP were used as they are referenced in the Turbomole 5.6 internal basis set library.

Conclusions

The treatment of (mes*)NHLi with $SeCl_4$ affords supermesityl selenium diimide (**1**) in a good yield. The molecule was found to exhibit an unprecedent *anti,anti*-conformation. This was deduced by an approximate crystal structure determination. Furthermore, the PBE0/TZVP calculations showed that the *anti,anti*-conformation is energetically most favourable, though the two other possible conformations lie close in energy**.** The ^{77}Se NMR spectrum could also be assigned in terms of the *anti,anti*-conformation.

By contrast, the analogous reaction involving mesityl amine unexpectedly lead to the reduction of selenium and afforded a novel mesityl selenium(II) diamide (**2**). The reaction products were characterized by X-ray crystallography and ^{77}Se and ^{13}C NMR spectroscopy. In solution, the molecule shows the presence of both *syn*- and *anti*-isomers, but only the *anti*-isomer is isolated in the solid state.

The PBE0/TZVP calculations of the isotropic ^{77}Se shielding tensors were carried out on 28 molecules for which the ^{77}Se chemical shifts were unambiguously known. The computed shielding tensors exhibit a good linear relationship with the observed chemical shifts. The

calculated mean deviation between calculated and experimental chemical shifts amounts to 48 ppm for the 32 different chemical shifts. While the inclusion of solvent effects during geometry optimization would have improved the accuracy of the shielding tensor calculations, it would be time-consuming. For the semi-quantitative purposes that are aimed at the assignment of experimental ^{77}Se chemical shifts, the present method provides sufficient accuracy. This is demonstrated by the successful assignment of the observed ^{77}Se chemical shifts to the *anti,anti*-isomer of Se{N(mes*)}$_2$, and *syn*- and *anti*-isomers of Se{NH(mes)}$_2$

Acknowledgements

Financial support from Academy of Finland, Finnish Cultural Foundation, Ministry of Education in Finland, and NSERC (Canada) is gratefully acknowledged.

References

1. K. B. Sharpless, T. Hori, L. K. Truesdale, C. O. Dietrich, *J. Am. Chem. Soc.* **1976**, *98*, 269.
2. K. Vrieze, G. van Koten, *Recl. Trav. Chim. Pays-Bas* **1980**, *99*, 145.
3. T. Chivers, R. W. Hilts, *Coord. Chem. Rev.* **1994**, *137*, 201.
4. A. F. Hill, *Adv. Organomet. Chem.* **1994**, *36*, 159.
5. R. Bussas, G. Kresze, H. Münsterer, A Schwöbel, *Sulfur Rep.* **1983**, *2*, 215.
6. J. Konu, A. Maaninen, K. Paananen, P. Ingman, R. S. Laitinen, T. Chivers, *Inorg. Chem.* **2002**, *41*, 1430, and references therein.
7. M. Herberhold, W. Jellen, *Z. Naturforsch.* **1986**, *41b*, 144.
8. B. Wrackmeyer, B. Distler, S. Gerstmann, M. Herberhold, *Z. Naturforsch.* **1993**, *48b*, 1307.
9. F. Fockenberg, A. Haas, *Z. Naturforsch.* **1986**, *41b*, 413.
10. G. Li, H.-T. Chang, K. B. Sharpless, *Angew. Chem., Int. Ed. Engl.* **1996**, *35*, 451.
11. J. Gindl, M. Björgvinsson, H. W. Roesky, C. Freire-Erdbrügger, G. M. Sheldrick, *J. Chem. Soc., Dalton Trans.* **1993**, 811.
12. T. Chivers, M. Parvez, G. Schatte, *Inorg. Chem.* **1996**, *35*, 4094.
13. H. M. Tuononen, R. J. Suontamo, J. U. Valkonen, R. S. Laitinen, T. Chivers, *Inorg. Chem.* **2003**, *42*, 2447, and references therein.
14. T. Maaninen, R. Laitinen, T. Chivers, *Chem. Commun.* **2002**, 1812.
15. T. Chivers, X. Gao, M. Parvez, *J. Chem. Soc., Dalton Trans.* **1994**, 2149.
16. T. Chivers, X. Gao, M. Parvez, *J. Am. Chem. Soc.* **1995**, *117*, 2359.
17. T. Chivers, X. Gao, M. Parvez, *Inorg. Chem.* **1996**, *35*, 9.
18. N. Sandblom, T. Ziegler, T. Chivers, *Inorg. Chem.* **1998**, *37*, 354.

19. S. K. Bestari, A. W. Cordes, R. T. Oakley, K. M. Young, *J. Am. Chem. Soc.* **1990**, *112*, 2249.

20. T. Maaninen, H. M. Tuononen, G. Schatte, R. Suontamo, J. Valkonen, R. Laitinen, T. Chivers, *Inorg. Chem.* **2004**, *43*, 2097.

21. R. O. Duthaler and J. O. Roberts, *J. Am. Chem. Soc.* **1978,** *100*, 4969.

22. M. Bjorgvinnsson, H. W. Roesky, F. Paver, D. Stalke, *Inorg. Chem.* **1990**, *29*, 5140.

23. I. Ya. Bagryanskaya, Y. V. Gatilov, A. V. Zibarev, *Mendeleev. Comm.*, **1999**, 157.

24. G. Schreckenbach, Y. Ruiz-Morales, T. Ziegler, *J. Chem. Phys.* **1996**, *104*, 8605.

25. M. Bühl, W. Thiel, U. Fleischer, W. Kutzelnigg, *J. Phys. Chem.* **1995**, *99*, 4000.

26. W. Nakanishi, H. Satoko, *J. Phys. Chem. A* **1999**, *103*, 6074, and references therein.

27. R. Laitinen, T. Pakkanen, *J. Chem. Soc. Chem. Commun.* **1986**, 1381.

28. T. Maaninen, T. Chivers, R. Laitinen, E. Wegelius, *Chem. Commun.* **2000**, 759.

29. R. C. Burns, M. J. Collins, R. J. Gillespie, G. J. Schrobilgen, *Inorg. Chem.* **1986**, *25*, 4465.

30. G. M. Sheldrick, *SHELXS-97, Program for the Solution of Crystal Structures*; University of Göttingen, Göttingen, Germany 1997.

31. G. M. Sheldrick, *SHELXL97-2, Program for the Solution of Crystal Structures*; University of Göttingen, Göttingen, Germany 1997.

32. J. P. Perdew, K. Burke, M. Ernzerhof, *Phys. Rev. Lett.* **1996**, *77*, 3865; ibid. **1997**, *78*, 1396 (E).

33. J. P. Perdew, M. Ernzerhof, K. Burke, *J. Chem. Phys.* **1996**, *105*, 9982.

34. C. Adamo, V. Barone, V. *J. Chem. Phys.* **1999**, *110*, 6158.

35. C. Adamo, V. Barone, V., *Chem. Phys. Letters* **1998**, *298*, 113.

36. C. Adamo, V. Barone, V., V., *J. Mol. Struct.* (*Theochem)* **1999**, *493*, 145.

37. C. Adamo, V. Barone, V., *Theor. Chem. Acc.* **2000**, *105*, 169.

38. T. Maaninen, T., Chivers, R. Laitinen, G. Schatte, M. Nissinen, *Inorg. Chem.* **2000**, *39*, 5341.

39. R. Ditchfield, *Mol. Phys.* **1974**, *27*, 789.

40. TURBOMOLE, Program Package for *ab initio* Electronic Structure Calculations, Version 5.6. R. Ahlrichs, *et al.* Theoretical Chemistry Group, University of Karlsruhe, Karlsruhe, Germany, 2002.

41. O. Treutler, O., R. Ahlrichs, *J. Chem. Phys.* **1995**, *102*, 246.

42. M. V. Arnim, R. Ahlrichs, *J. Comp. Chem.* **1998**, *19*, 1746.

43. M. J. Frisch, G. W. Trucks, H. B. Schlegel, G. E. Scuseria, M. A. Robb, J.R. Cheeseman, J. A. Montgomery, Jr., T. Vreven, K. N. Kudin, J. C. Burant, J. M. Millam, S. S. Iyengar, J. Tomasi, V. Barone, B. Mennucci, M. Cossi, G. Scalmani, N. Rega, G. A. Petersson, H. Nakatsuji, M. Hada, M. Ehara, K. Toyota, R. Fukuda, J. Hasegawa, M. Ishida, T. Nakajima, Y. Honda, O. Kitao, H. Nakai, M. Klene, X. Li, J. E. Knox, H. P. Hratchian, J. B. Cross, C. Adamo, J. Jaramillo, R. Gomperts, R. E. Stratmann, O. Yazyev, A. J. Austin, R. Cammi, C. Pomelli, J. W. Ochterski, P. Y. Ayala, K. Morokuma, G. A. Voth, P. Salvador, J. J. Dannenberg, V. G. Zakrzewski, S. Dapprich, A. D. Daniels, M. C. Strain, O. Farkas, D. K. Malick, A. D. Rabuck, K. Raghavachari, J. B. Foresman, J. V. Ortiz, Q. Cui, A. G. Baboul, S. Clifford, J. Cioslowski, B. B. Stefanov, G. Liu, A. Liashenko, P. Piskorz, I. Komaromi, R. L. Martin, D. J. Fox, T. Keith, M. A. Al-Laham, C. Y. Peng, A. Nanayakkara, M. Challacombe, P. M. W. Gill, B. Johnson, W. Chen, M. W. Wong, C. Gonzalez, and J. A. Pople, Gaussian 03, (Revision B.04), Gaussian, Inc., Pittsburgh, PA, 2003.

Table 1. Selected experimental and PBE0/TZVP optimized bond parameters of $Se\{NH(mes)\}_2 \cdot 2(mes)NH_2$.

Parameter	Crystal structure	PBE0/TVZP	
		syn-isomer	*anti*-isomer
Se1-N1 (Å)	1.847(3)	1.854	1.850
Se1-N2 (Å)	1.852(3)	1.854	1.850
N1-C11 (Å)	1.421(4)	1.409	1.410
N2-C21 (Å)	1.421(4)	1.409	1.410
N1-H1 (Å)	0.75(5)	1.009	1.009
N2-H2 (Å)	0.81(4)	1.009	1.008
N1-Se1-N2 (deg.)	109.9(1)	109.5	111.8
Se1-N1-C11 (deg.)	121.7(2)	123.7	125.8
Se1-N1-H1 (deg.)	109(4)	110.0	111.6
Se1-N2-C21 (deg.)	120.2(2)	123.7	125.8
Se1-N2-H2 (deg.)	108(2)	110.0	111.6
C11-N1-H1 (deg..)	113(4)	112.6	113.4
C21-N2-H2 (deg..)	118(3)	112.6	113.4
N1-Se1-N2-C21 (deg.)	65.4(3)	72.1	61.1
N1-Se1-N2-H2 (deg.)	-76(3)	-72.2	-76.4
N2-Se1-N1-C11 (deg.)	64.6(3)	-72.1	61.1
N2-Se1-N1-H1 (deg.)	-69(4)	72.2	-76.4

Table 2. Calculated PBE0/TZVP(P)//PBE0/TZVP and experimental ^{77}Se NMR chemical shifts of selected selenium compounds

molecule		$\sigma_{iso.}$	$\delta_{calc.}$	$\delta_{exptl.}$	$\delta_{diff.}$
SeH_2		2153	-290	-345 [a]	55
$SeMe_2$		1824	40	0	40
MeSeH		1973	-110	-155 [a]	45
$SeMe_3^+$		1572	292	253 [a]	39
MeSeSeMe		1542	321	281 [a]	40
Me_2SeCl_2		1440	424	448 [a]	-24
SeF_6		1175	688	631 [b]	57
Me_2SeO		1061	802	812 [a]	-10
F_2SeO_2		864	1000	948 [a]	52
SeF_4		710	1153	1083 [a]	70
F_2SeO		461	1402	1378 [a]	24
Se_6		1140	723	685 [c]	38
Se_8		1209	655	615 [c]	40
SeCO		2341	-478	-447 [b]	-31
SeC^tBu_2		-354	2217	2131 [b]	86
$Se(SiH_3Si)_2$		2460	-597	-666 [b]	69
^{t}BuN(SeCl)$_2$		18	1846	1786 [d]	60
s,a-Se(N^{t}Bu)$_2$		167	1696	1653 [e]	43
s,a-Se(NAd)$_2$		171	1692	1651 [f]	41
Se[(NSiMe$_3$)$_2$]$_2$		755	1108	1130 [e]	-22
OSe(μ-N^{t}Bu)$_2$SeO		719	1144	1242 [g]	-98
OSe(μ-NAd)$_2$SeO		732	1131	1213 [g]	-82
^{t}BuNSe(μ-N^{t}Bu)$_2$SeO	Se=N	1002	861	882 [d]	-21
	Se=O	737	1127	1157 [d]	-30
^{t}BuNSe(μ-N^{t}Bu)$_2$SO$_2$		1088	776	824 [d]	-48
Se$_3$(N^{t}Bu)$_2$	NSeN	310	1553	1626 [d]	-73
	SeSe	686	1177	1183 [d]	-6
Se$_3$(N^{t}Bu)$_3$		573	1291	1396 [d]	-105
Se$_6$(N^{t}Bu)$_2$	N**Se**Se	762	1101	1109 [d]	-8
	Se**Se**Se	1233	631	518 [d]	113
Se$_9$(N^{t}Bu)$_6$	NSeN	465	1398	1425 [d]	-27
	NSeSeN	626	1238	1203 [d]	35

[a] Ref. 26, and references therein. [b] Ref. 24, and references therein. [c] Ref. 27 [d] Ref. 28. [e] Ref. 8. [f] Ref. 14. [g] Ref. 20.

Table 3. Calculated PBE0/TZVP(P)//PBE0/TZVP and experimental ^{77}Se NMR chemical shifts of Se{N(mes*)}$_2$ and Se{NH(mes)}$_2$.

Molecule		$\sigma_{iso.}$	$\delta_{calc.}$	$\delta_{exptl.}$	$\delta_{diff.}$
Se{N(mes*)}$_2$	*anti,anti*	-212	2076	1844	232
	syn,anti	1997	1666		
	syn,syn	622	1242		
Se{NH(mes)}$_2$	*anti*	796	1067	1077	-10
	syn	799	1066	1076	-10

Table 4. Details of structure determination of Se{NH(mes)}$_2$·2(mes)NH$_2$ at 150 K.[a]

	(mesNH)$_2$Se·2(mes)NH$_2$
formula	$C_{36}H_{50}N_4Se$
fw	617.76
crystal system	triclinic
space group	$P\bar{1}$ (NO. 2)
a, Å	8.413(2)
b, Å	14.012(3)
c, Å	14.902(3)
α, deg.	73.81(3)
β, deg.	89.34(3)
γ, deg.	83.10(3)
U, Å^3	1674.3(6)
Z	2
$\rho_{calc.}$ g cm^{-3}	1.225
μ(MoKα), mm^{-1}	1.151
F(000)	656
crystal size (mm^3)	0.15 x 0.10 x 0.10
reflections collected	29086
unique reflections	6571
observed reflections	5864
R_{INT}	0.0711
R_1 [b] [$I \geq 2\sigma(I)$]	0.0513
wR_2 [c] [$I \geq 2\sigma(I)$]	0.1395

R_1 [b] (all data)	0.0584
wR_2 [c] (all data)	0.1455
GOF on F^2	1.021
$(\Delta\rho)_{max}$, e^- Å^{-3}	0.565
$(\Delta\rho)_{min}$, e^- Å^{-3}	-0.588

[a] CCDC 244552 contains the supplementary crystallographic data for this paper. These data can be obtained free of charge via www.ccdc.cam.ac.uk/conts/retrieving.html (or from the CCDC, 12 Union Road, Cambridge CB2 1EZ, UK; fax: +44 1223 336033; e-mail: deposit@ccdc.cam.ac.uk). [b] $R_1 = [\Sigma||F_o|-|F_c||]/[\Sigma|F_o|]$. [c] $wR_2 = \{[\Sigma w(F_o^2-F_c^2)^2]/[\Sigma w(F_o^2)^2]\}^{½}$

Figure Captions

Figure 1. The optimized PBE0/TZVP geometries of (a) *anti,anti*-Se{N(mes*)}$_2$, (b) *syn,anti*-Se{N(mes*)}$_2$, and (c) *syn,syn*-Se{N(mes*)}$_2$ indicating selected bond parameters. The experimental values from a tentative crystal structure determination of the *anti,anti*-isomer are shown in italics. Carbon atoms are indicated as solid gray (or white), nitrogen atoms with horizontal stripes, and the selenium atom with diagonal stripes.

Figure 2. The crystal structure of Se{NH(mes)}$_2$·2(mes)NH$_2$ indicating the numbering of the atoms. The thermal ellipsoids are drawn at 50 % probability level.

Figure 3. Two possible isomers of Se{NH(mes)}$_2$ that are for convenience referred to as (a) *syn*-isomer and (b) *anti*-isomer. Carbon atoms are indicated as solid gray (or white), nitrogen atoms with horisontal stripes, and the selenium atom with diagonal stripes.

Figure 4. The linear regression line of the isotropic shielding tensors as a function of experimental ^{77}Se chemical shifts.

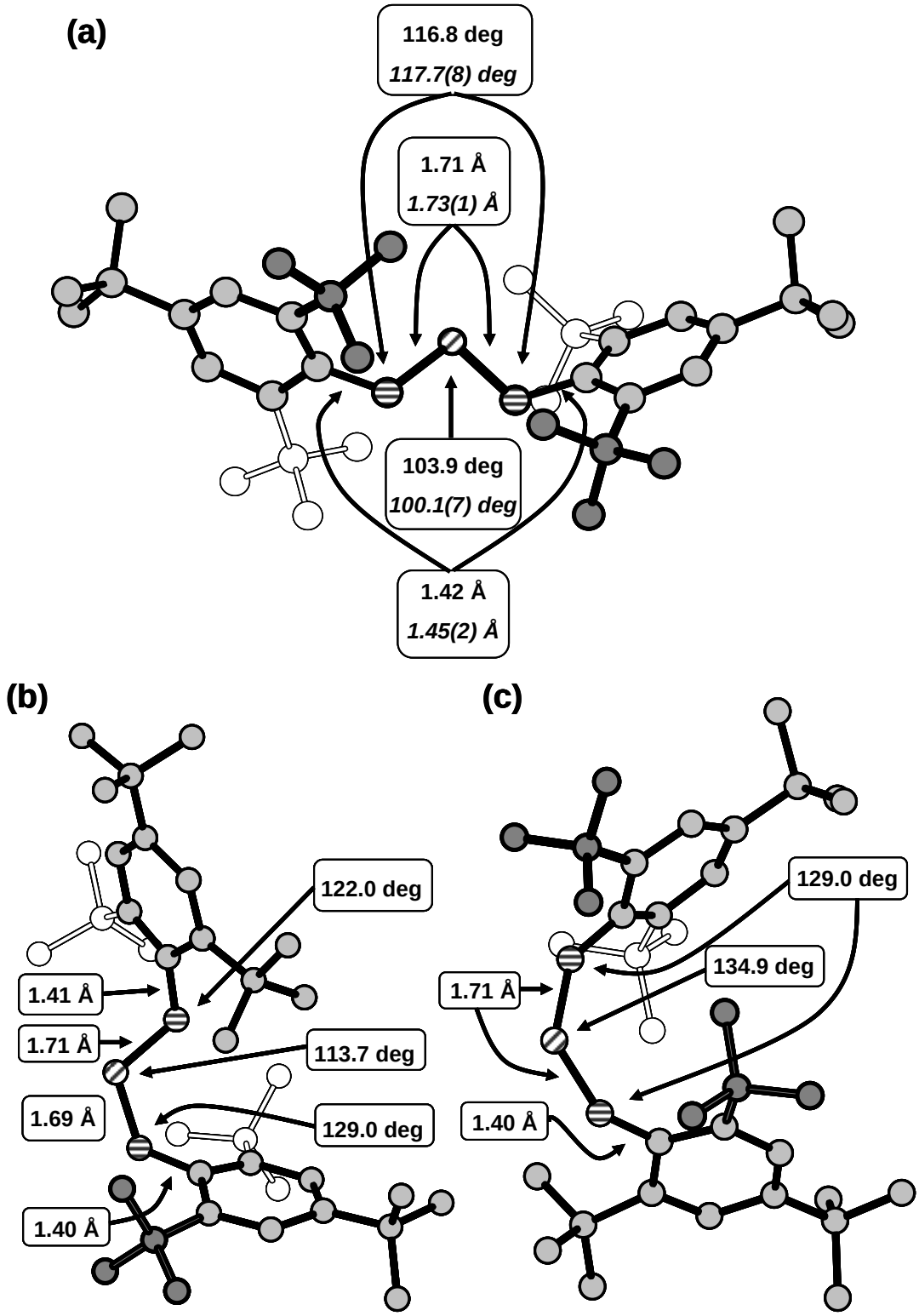
(a)
116.8 deg
117.7(8) deg
1.71 Å
1.73(1) Å
103.9 deg
100.1(7) deg
1.42 Å
1.45(2) Å
(b)
122.0 deg
1.41 Å
1.71 Å
113.7 deg
1.69 Å
129.0 deg
1.40 Å
(c)
129.0 deg
134.9 deg
1.71 Å
1.40 Å

Figure 1

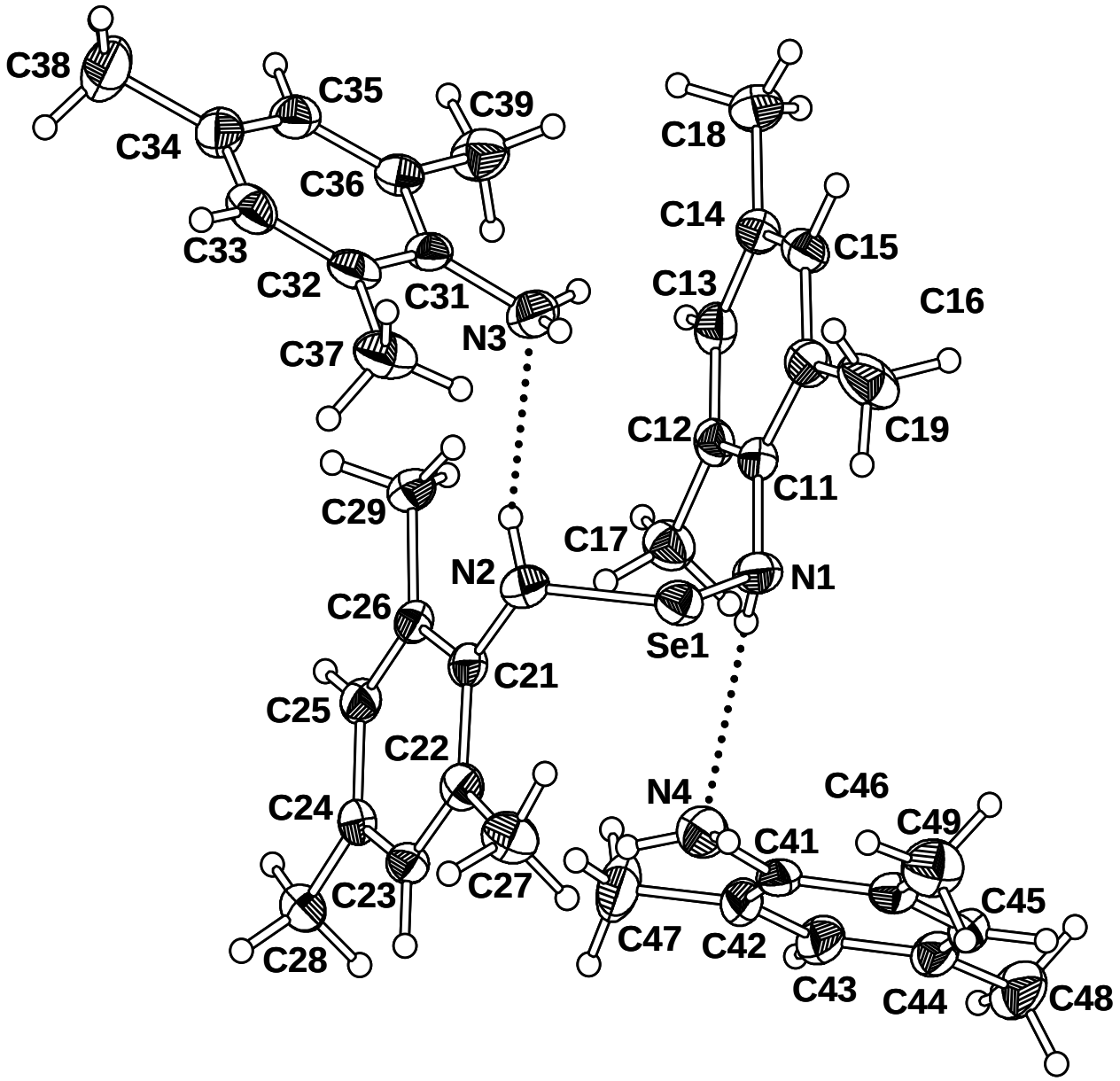
C38
C35
C39
C34
C36
C33
C32
C31
N3
C37
C29
C26
N2
C21
C25
C22
C24
C23
C27
C28
C18
C14
C15
C13
C16
C12
C19
C11
C17
N1
Se1
N4
C46
C49
C41
C45
C47
C42
C43
C44
C48

Figure 2

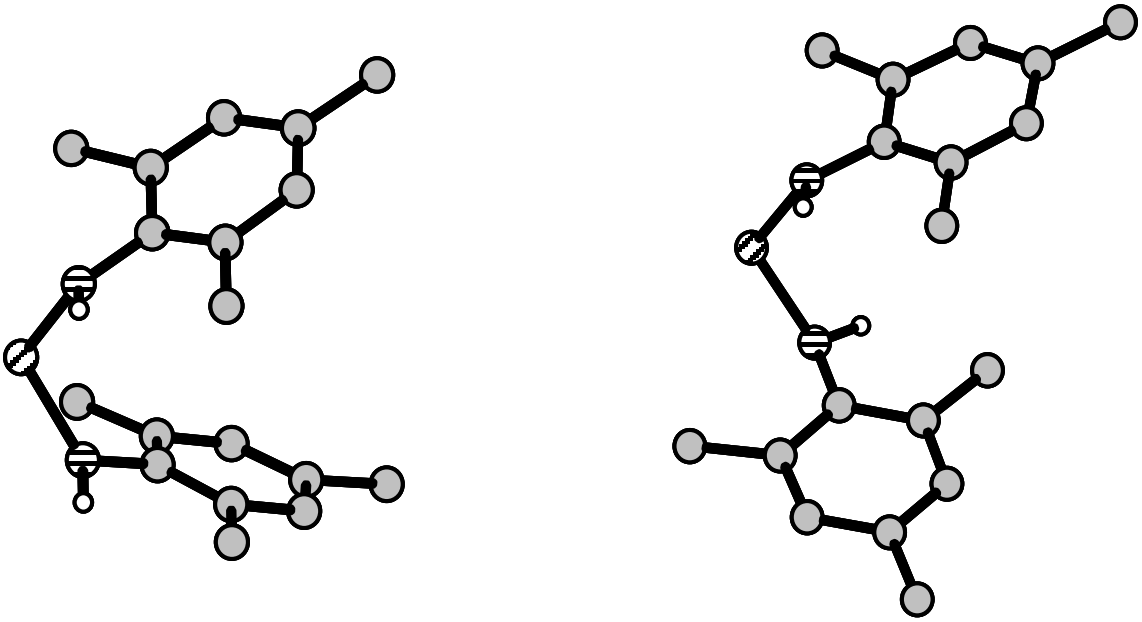

Figure 3

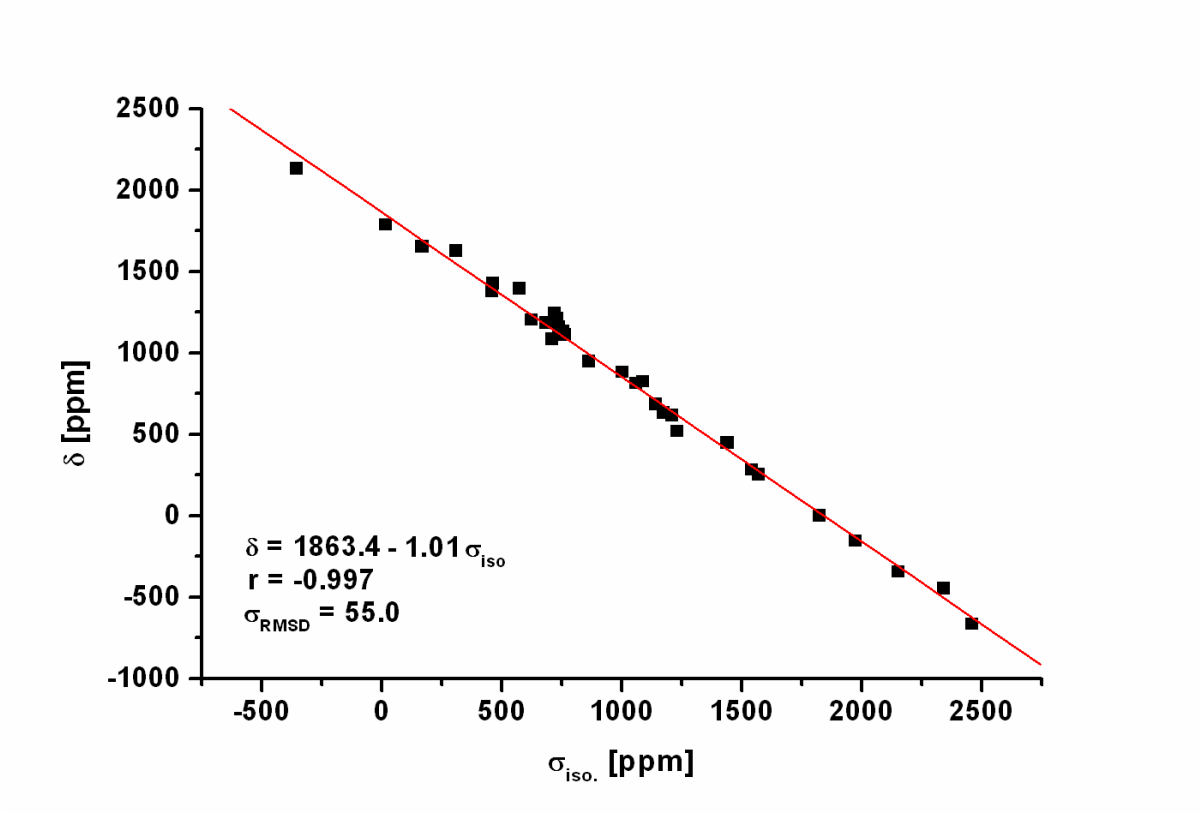
2500
2000
1500
1000
500
0
-500
-1000
δ [ppm]
-500
0
500
1000
1500
2000
2500
σiso. [ppm]
δ = 1863.4 - 1.01 σiso
r = -0.997
σRMSD = 55.0

Figure 4